Retrievals of Precipitable Water Vapor and Aerosol Optical Depth from direct sun measurements with EKO MS711 and MS712 Spectroradiometers

Congcong Qiao[1,2], Song Liu[1,2], Juan Huo[1], Xihan Mu[3], Ping Wang[4], Shengjie Jia[5], Xuehua Fan[1],
Minzheng Duan[1,2*]

[1]LAGEO, Institute of Atmospheric Physics, Chinese Academy of Sciences, Beijing, 100029, China
[2]College of Earth and Planetary Sciences, University of Chinese Academy of Sciences, Beijing, 100049, China
[3]State Key Laboratory of Remote Sensing Science, Beijing Normal University, Beijing, 100875, China
[4] Royal Netherlands Meteorological Institute (KNMI), De Bilt, the Netherlands
[5]Beijing Keytec Technology Co., Ltd., Beijing, 100102, China

Correspondence to: Minzheng Duan (dmz@mail.iap.ac.cn)

Abstract. Based on the strict radiative transfer algorithm, a new method is developed to derive the Precipitable Water Vapor (PWV) and Aerosol optical depth (AOD) from the ground-based measurements of direct sun irradiance. The attenuated direct irradiance from 300 nm to 1700 nm was measured by a pair of grating spectroradiometers MS711 and MS712 produced by EKO INSTRUMENTS, located at the Institute of Atmospheric Physics (IAP), Chinese Academy of Sciences (39.98° N, 116.38° E), from June 2020 to March 2021. The PWV and AOD inversion results obtained by MS711 and MS712 are compared with the synchronous data of CE-318, which shows that the two retrieval results are highly consistent. The correlation coefficient, mean bias and standard deviation of PWV_{EKO} and PWV_{CIMEL} are 0.999, -0.027 cm (-3.57 %) and 0.054 cm (3.93 %) respectively, and the relative deviations of the differences between the two are slightly larger for drier air (PWV<5 mm) and lower solar elevation angle. The correlation coefficients of AOD_{EKO} and AOD_{CIMEL} at 380, 440, 500, 675, 870, 1020 nm are greater than 0.99, and the relative deviations vary between -13.59 % and 9.37 %. Compared with regular sun photometers such as CE-318 and POM, a strong water vapor absorption band around 1370 nm is introduced. Furthermore, an inversion test was performed to verify that the band near 1370 nm is more suitable than 940 nm to retrieve PWV in a relatively dry atmosphere.

1 Introduction

Water vapor and aerosols are two key components of the atmosphere (Bojinski et al., 2014; IPCC, 2013), and the current accuracy of their indirect measurements from spaceborne instruments (Dubovik et al., 2019; Kaufman et al., 2002; Kokhanovsky, 2013) are unsatisfactory in evaluation of earth climate simulations and environment modelling (IPCC, 2021), often needing to be combined with ground-based measurements for higher accuracy retrievals (Li et al., 2019; WMO, 2016).

30 As for PWV, ground observation methods include Global Positioning System (GPS), MicroWave radiation Profiler System (MWPS), sun photometers (CE-318, POM, MFR), etc. GPS signals delayed by atmosphere can be used to obtain global PWV at a relatively high temporal resolution, but the algorithm still needs to be improved for accuracy (Bevis et al., 1992; Wang et al., 2007). MWPS measures the microwave radiation emitted from the atmosphere, yields a vertical profile of water vapor, which can then be integrated to derive PWV (Güldner and Spänkuch, 2001; J. and Güldner, 2013). The advantages of

35 using microwave for PWV is that aerosols have little effect, but the disadvantage is that this kind of instruments is generally very expensive. Sun photometers are easy to operate and economical to build observation network (Augustine et al., 2008; Wehrli, 2003), so they are widely used to monitor water vapor and aerosols (Barreto et al., 2014; Cuevas Agulló et al., 2015; Kazadzis et al., 2014; Schmid et al., 1999). Among them, the CE-318 produced by French CIMEL corporate is the most popular one and used in the Aerosol Robotic NETwork (AERONET) project (Holben et al., 1998), China Aerosol Remote

40 Sensing Network (CARSNET) (Che et al., 2016), and Sun–Sky Radiometer Observation Network (SONET) (Li et al., 2018) etc. Similar instruments such as POM are deployed in the SKY radiometer NETwork (SKYNET) (Campanelli et al., 2012; Campanelli et al., 2014).

Currently, AERONET is the most recognized ground-based aerosol observation network. Since the 1990s, NASA and PHOTONS have established more than 500 sites worldwide based on CE-318 sun photometer, which could provide water

45 vapor and aerosol optical properties through the measurements in the visible and short-wave infrared band. The aerosol and PWV products derived from CE-318 are often used as reference to validate those obtained by other methods. Additionally, some scientists have attempted to retrieve PWV and AOD using spectral measurements. Estellés et al. (2006) used li-COR 1800 spectroradiometer to retrieve AOD, their results showed the differences with those from CE-318 of 0.01-0.03 and 0.02-0.05 in the ultraviolet and visible band, respectively. Cachorro et al. (2009) compared AOD obtained by li-COR and sun

50 photometer and found the differences of AOD within 0.02 in the spectral range of 440-1200 nm. The results of PWV and AOD from spectral measurements of Precision Solar spectroRadiometer (PSR) showed a standard deviation of 0.18 cm for PWV and an overestimation of 0.01-0.03 for AOD compared to CE-318, and the PWV given by the integration of single water vapor band near 940 nm has great variability at different wavelengths (Kazadzis et al., 2018a; Kazadzis et al., 2018b; Kazadzis et al., 2014; Raptis et al., 2018). García et al. (2020;2021) retrieved PWV and AOD using the EKO MS711

55 spectroradiometer at Izana Observatory in Spain, and compared them with CE-318, showing that PWV has a mean bias of 0.033 cm, and the AOD is basically consistent.

A method of simple Lambert-Beer law was used to retrieve AOD and a three-parameter formula proposed by Ingold et al. (2000) was used to retrieve PWV with measurements of 940 nm water vapor band in the above mentioned publications. Since the three-parameter formulation method is very sensitive to the instrument slit function, air quality and wavelength, a

60 spectral fitting algorithm is proposed to derive the PWV. In this work, Direct Normal solar Irradiance (DNI) at 300-1700 nm was measured with EKO MS711 and MS712 spectroradiometers, then AOD and PWV were retrieved and compared to those of CE-318. In addition, the water vapor absorption band near 1370 nm was also used to obtain PWV, which was expected to improve the water vapor retrieval efficiency in dry environment.

2 Instruments

65 The grating spectroradiometers MS711 and MS712 are designed and developed by EKO INSTRUMENTS and can be used to measure the attenuation of direct solar beams in the range of 300-1700 nm, with a high time resolution of 1 minute. The Full Width at Half Maximum (FWHM), wavelength accuracy, full Field Of View (FOV) angle and exposure time of the two spectroradiometers are the same, in order of < 7 nm, ±0.2 nm, 5° and 10-5000 ms. The differences between the two are that the average wavelength interval is 0.4 nm and 2.0 nm, respectively, and the temperature control is 25±2 ℃ and -5±0.5 ℃,

70 respectively. The main specifications related to MS711 and MS712 are listed in Table 1.

Table 1 EKO MS711 and MS712 spectroradiometers specifications

Sensor	MS711	MS712
Wavelength	300-1100 nm	900-1700 nm
Wavelength Interval	0.3-0.5 nm	1.2-2.2 nm
Temperature Control	25±2 ℃	-5±0.5 ℃
Dome material	Synthetic Quartz	BK7
Operating conditions	Tem: 0~+40 ℃, Humidity: 0~90 %RH*No condensation	
Spectral Resolution	<7 nm	
Wavelength Accuracy	±0.2 nm	
Exposure Time	10-5000 ms	
Communication	RS-422 / 232C	
Power supply	100-240 VAC, 50/60 Hz	
Field of view (FOV)	5°	

CE-318 is a narrow-band sun photometer developed by CIMEL Electronique in France, which can directly measure the

75 radiance of the sun and the sky. Measurements are usually made every 10-15 minutes at 340, 380, 440, 500, 675, 870, 940, 1020 and 1640 nm through rotating filter wheels. The spectral resolution of the instrument is 2 nm, 10 nm and 40 nm in the ultraviolet band, visible band and near-infrared band (Schmid et al., 1999), respectively. The FOV of CE-318 is about 1.2° and calibrated annually.
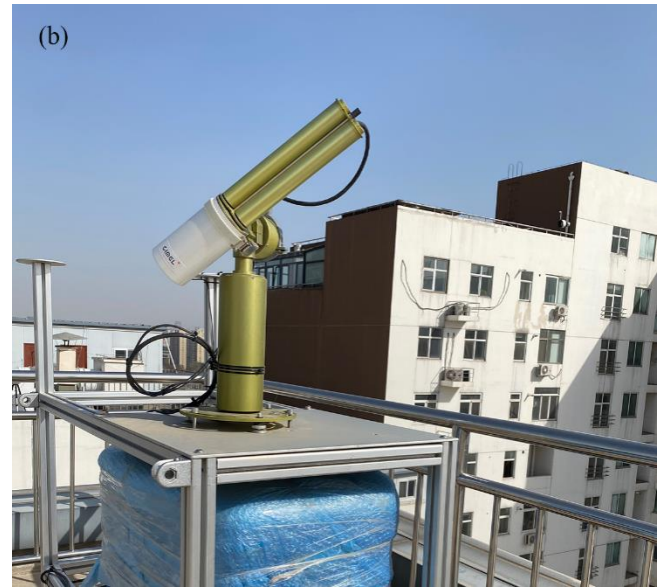
Figure 1. The EKO spectroradiometers (a) and CE-318 photometer (b) are collocated at the top of IAP's building.

The instruments are collocated in the Institute of Atmospheric Physics (IAP), Chinese Academy of Science (CAS), Beijing (39.98° N, 116.38° E, 92 m a.s.l, Fig. 1), located in a relatively dry area in northern China, where most precipitation occurs in summer, and the water vapor content in the atmosphere of other seasons are very low. The data used here are collected from June 2020 to March 2021, and level 1.5 data of AERONET (https://AERONET.gsfc.nasa.gov/) are used for comparison.

3 Inversion Method

3.1 Cloud screening

Cloud contamination need to be avoided before performing the inversion. Considering that the change of clouds in a short time are usually more drastic than that of aerosols and the temporal resolution of EKO measurements is relatively high at 1 min. We referred to the methods proposed by Smirnov et al. (2000) and Michalsky et al. (2001) for cloud screening of ground-based measurements by imposing a threshold on the standard deviation of the measurements to extract the clear-sky portion of the dataset. Specifically, in order to implement cloud detection, if the standard deviation of the measured value of MS711 at 870 nm within 5 minutes is greater than $15 \ w \cdot m^2 \cdot \mu m^{-1}$, and the standard deviation of the measured value of MS712 at 1370 nm within 5 minutes is greater than $1 \ w \cdot m^2 \cdot \mu m^{-1}$, we label it as cloud contaminated.
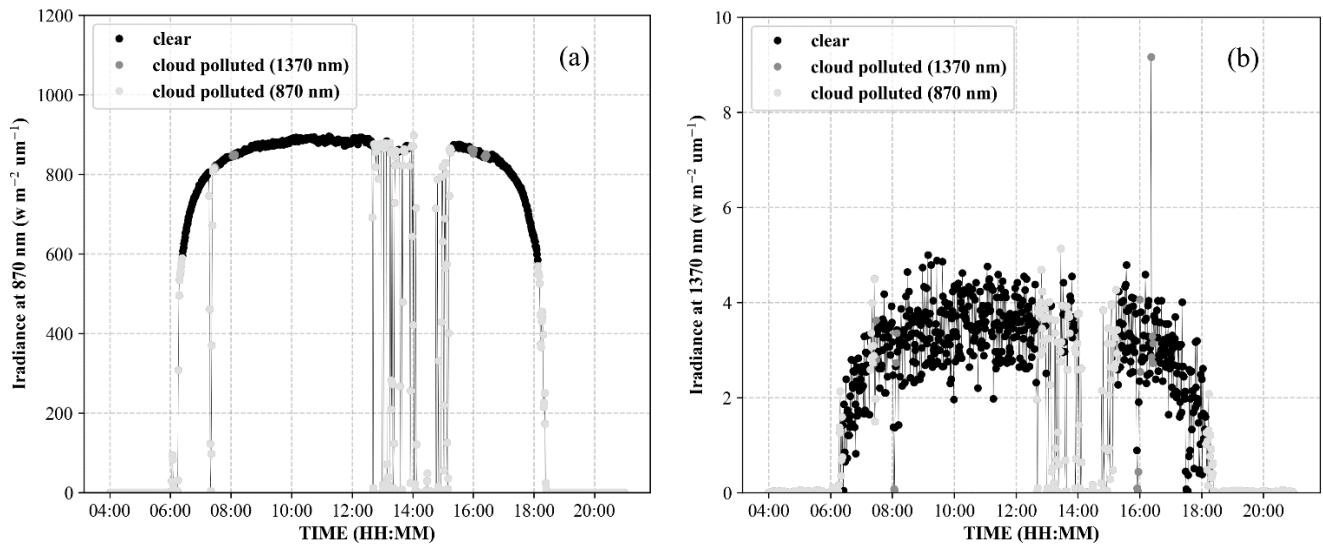
Figure 2. Direct normal irradiances measurements of EKO instruments at 870 nm (a) and 1370 nm (b) on 8 September 2020 at IAP. Cloudy parts and very small measurements are shown in grey, with light grey and dark grey filtered out using 870nm and 1370nm measurements respectively, and clear-sky parts shown in black.

Figure 2(a) and (b) represent the diurnal variations of the radiation measurements of MS711 at 870 nm and MS712 at 1370 nm on September 8, 2020, respectively. The light grey and dark grey points in the figure represent the data that may have cloud contamination filtered out by the cloud detection program. The light grey is the data filtered by the measurement value at 870 nm, and the dark grey is the data filtered by the measurement value at 1370 nm. As can be seen from the figure, the cloud screening effect of this method is quite good, but the current threshold is manually selected, which cannot completely exclude missed or false detection.

3.2 PWV inversion

Figure 3 shows the theoretical transmittance curves for Rayleigh scattering, aerosols, and water vapor from 300 nm to 1700 nm calculated by MODTRAN 4.3 (Larar et al., 1999) at 0° solar zenith angle. WMO (2005) recommends the use of 719, 817 and 946 nm central wavelengths to obtain PWV, which are marked with the grey arrows in Fig. 3. Ingold et al. (2000) compared the water vapor inversion results of these wavelengths and found that 946 nm is of the most suitable for PWV retrieval. The water vapor data provided by AERONET are also obtained by the band near 946 nm (Smirnov et al., 2004). However, as demonstrated in Fig. 3, the transmittance at 946 nm turns to be less sensitive to water vapor as the air becomes drier, while the water vapor absorption remains strong around 1370 nm, therefore, the water vapor absorption window of 1350-1450 nm was considered for PWV inversion in very dry atmosphere.
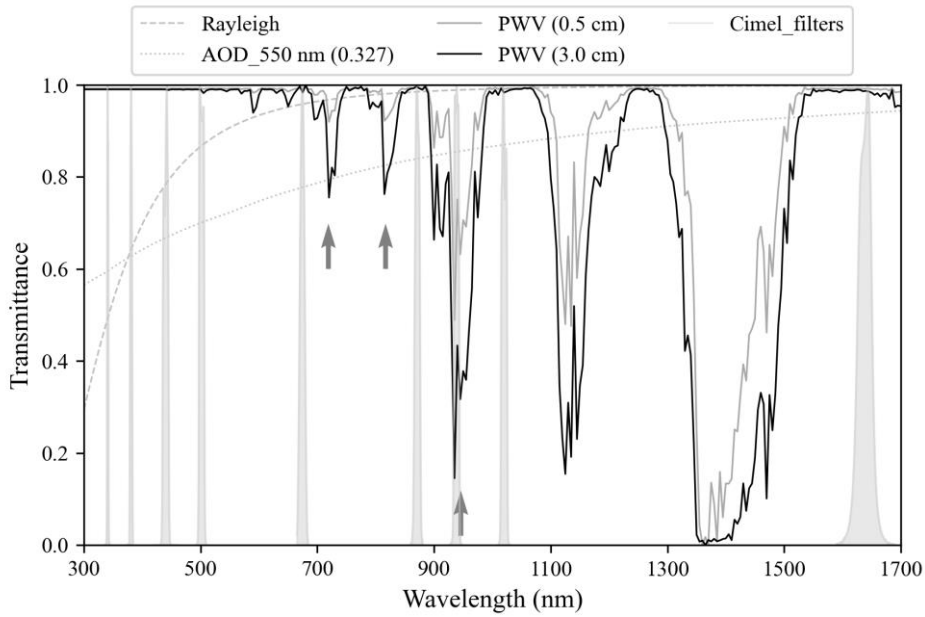
Figure 3. The spectrum response curves of CE-318 photometer's filter wheels, and the transmittance of water vapor, aerosols and Rayleigh scattering in the spectral range of 300–1700 nm, which are calculated by MODTRAN4.3 at SZA=0°, PWV=0.5 cm, PWV=3.0 cm and Boundary Aerosol Model=Rural extinction(spring-summer), VIS=23 km. The wavelengths pointed by the grey arrows represent WMO recommendations for PWV retrieval.

The transmittance $T(\lambda)$ of the whole atmosphere along the sun's direction can be expressed by the Bouguer-Lambert-Beer law (Swinehart, 1962):

$$T(\lambda) = \frac{I(\lambda)}{I_0(\lambda)} = e^{-m_r\tau_r(\lambda)-m_a\tau_a(\lambda)-m_g\tau_g(\lambda)} \ , \tag{1}$$

where $I(\lambda)$ is DNI recorded by the EKO instruments at wavelength λ, $I_0(\lambda)$ is the solar radiance at the top of the atmosphere, m and τ is the air mass and optical thickness, respectively, the subscripts r, a and g denote the contribution of Rayleigh, aerosols and other atmospheric gases, respectively (Bodhaine et al., 1999; Gueymard, 2001; Hansen and Travis, 1974). In the water vapor absorption band near 940 nm and 1370 nm, the absorption of other gases except water vapor can be neglected, the subscription g in above equation is replaced by w , which means water vapor, and Eq. (1) can be rewritten as:

$$\frac{I(\lambda)}{I_0(\lambda)} = e^{-m_r\tau_r(\lambda)-m_a\tau_a(\lambda)}T_w(\lambda) \ , \tag{2}$$

$$T_w(\lambda) = \frac{I(\lambda)}{I_0(\lambda)e^{-m_r\tau_r(\lambda)-m_a\tau_a(\lambda)}} = \frac{I(\lambda)}{I_1(\lambda)} \ , \tag{3}$$

where T_w is the transmittance within the water vapor band, $I_1(\lambda)$ is the radiance without water vapor absorption:

$$I_1(\lambda) = I_0(\lambda)e^{-m_r\tau_r(\lambda)-m_a\tau_a(\lambda)} \ , \tag{4}$$

In theory, a completely water vapor correction on the spectral curve can fill in the water vapor absorption valley in the measured spectrum. Therefore, the radiance after removing the water vapor absorption $I_1(\lambda)$ can be approximated by interpolating the baseline points outside of the water vapor band. As shown by the dashed line in Fig. 4, besides the

frequently used water vapor absorption band near 940 nm, we also consider using the band near 1370 nm to invert the water

135 vapor content in the dry atmosphere. The average water vapor transmittance within the water vapor band between λ_1 and λ_2 can be expressed as:

$$T_{w,\Delta\lambda} = \frac{1}{\Delta\lambda} \int_{\lambda_1}^{\lambda_2} \frac{I(\lambda)}{I_1(\lambda)} d\lambda , \tag{5}$$
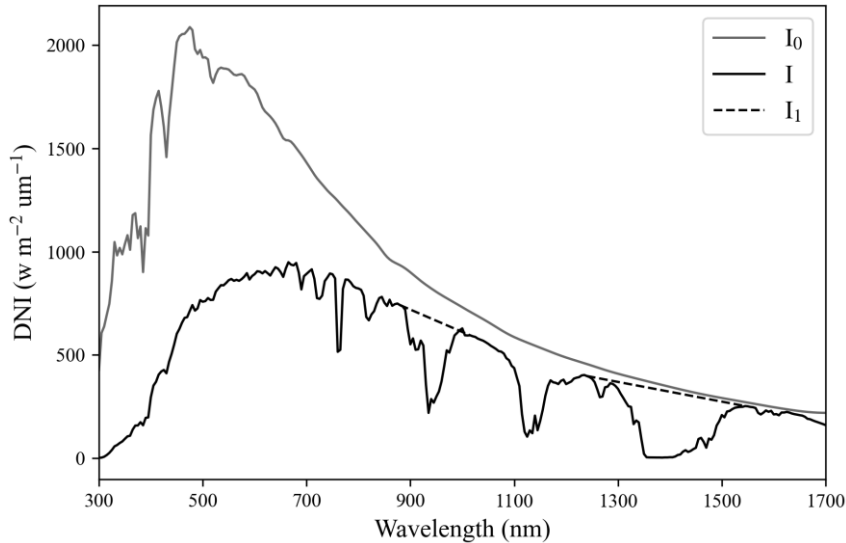
Figure 4. Direct normal solar irradiance reaching the surface (I), the solar irradiance at the top of the atmosphere (I_0), and the
140 **irradiance after approximately removing the water vapor absorption by interpolating the baseline points outside the water vapor band (I_1).**

$T_{w,\Delta\lambda}$ can be given either by EKO spectroradiometers MS711 and MS712 denoted as T_w^E, or by radiative transfer mode (MODTRAN version 4.3), denoted as T_w^M . In the mode calculations, ignoring aerosol, cloud, and other gas absorption, the input atmospheric profile is the 1976 US Standard Atmosphere, and the FWHM is set approximately equal to the EKO

145 instruments. The specific input parameters used in the calculations are listed in Table 2.

Table 2 The input parameters to the MODTRAN mode used in this work.

Parameters	Input parameters	References
Boundary Aerosol Model	No aerosol or cloud attenuation	——
Atmosphere profile	US Standard Atmosphere	NOAA (1976)
Altitude	0.05 km	——
Slit function	Gaussian function, with FWHM of 6.5 nm	——
Radiative transfer	DISORT	Stamnes et al. (1988)
Solar flux	0.1 nm resolution	Kurucz (1994)

T_w^M was simulated with first guess of PWV and then the differences between T_w^M and T_w^E was calculated:

150    $\Delta = T_w^E - T_w^M$,   (6)

Recalculating Eq. (6) by increasing or decreasing PWV depending on that Δ is positive or negative, the final value of PWV is given by iteration of Eq. (6) as Δ becomes smaller than a criteria value:

$$\Delta \to min\left(\left|T_{w,\Delta\lambda}^E - T_{w,\Delta\lambda}^M\right|\right) \Longrightarrow PWV \ ,$$ (7)

The PWV retrieval efficiency of BAND1 (900-990 nm) and BAND2 (1350-1450 nm) was tested separately using 1000 test
155   spectral curves generated by dint of MODTRAN simulations. In the mode simulations, the 1976 US standard atmospheric was used with random PWV between 0-0.5 cm, and solar zenith angle between 0°-30°, regardless of cloud and aerosol, and generating 1000 simulated spectral curves. Then the simulated spectral curves were superimposed with random noise of ±5 % at each wavelength to generate the test spectral curves. Figure 5 shows the results of the inversion test of the two bands, the PWV retrievals of the band near 1370 nm are closer to the input PWV when the spectrum is simulated, and it is more stable,
160   which demonstrates that the band around 1370 nm may be more suitable for water vapor retrieval in dry atmosphere than the band around 940 nm.
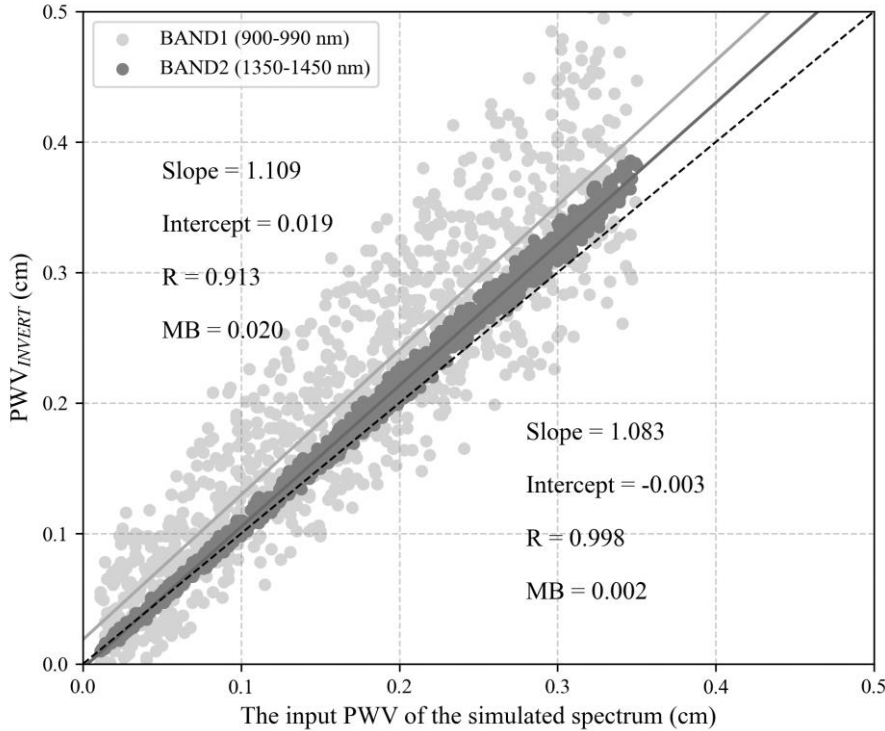
Figure 5. Scatter plot of the water vapor retrievals obtained from BAND1 and BAND2 of the test spectrum versus the input PWV of the simulated spectrum and their linear fits.

165   **3.3 AOD inversion**

After PWV is given, the spectral variation of AOD is derived according to Bouguer-Lambert-Beer law:

$$AOD = ln(I_0(\lambda)) - ln(I(\lambda)) - \tau_r - \tau_g , \tag{8}$$

$$\tau_r = p/p_0 \times 0.0088\lambda^{-4.05} , \tag{9}$$

$$\tau_g = \tau_{H_2O} + \tau_{N_2O} + \tau_{O_2} + \tau_{O_3} + \cdots , \tag{10}$$

170 To mitigate the absorption of gases other than water vapor, the wavelengths used for AOD inversion were carefully selected by using MODTRAN to calculate and filter the wavelengths corresponding to the transmittances greater than 0.999 that do not include Rayleigh scattering and continuous water vapor absorption. The AOD of other wavelengths were obtained by high-order fitting, specifically, as shown in Fig. 6. The Rayleigh scattering τ_r is given by Eq. (9) (Ramachandran et al., 1994), p_0=1013.25 hPa, p is provided by meteorological observation located in IAP, τ_{H_2O} is obtained from PWV inversion 175 as Sect. 3.2.
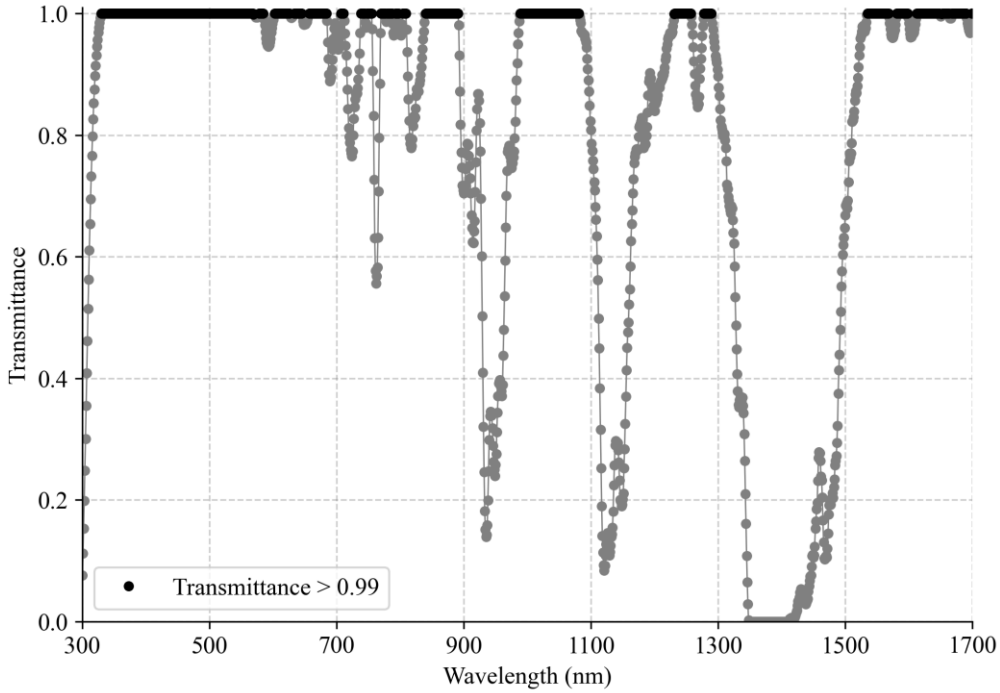
Figure 6. The transmittance without Rayleigh scattering and continuous water vapor absorption in the EKO band simulated by MODTRAN, where the transmittance value greater than 0.999 is marked in black, and the rest are marked in grey.

4 Uncertainty estimation of PWV and AOD retrievals

180 From the inversion method described in Sect. 3, it can be seen that the uncertainty of the inversion is mainly due to the uncertainty of the spectral measurements of the EKO instruments and the uncertainty of the retrieval algorithm. To estimate the uncertainty of the retrievals, 1000 spectrums were generated by randomly superimposing the calibration uncertainty (Table 3) at each wavelength of two spectral curves (measured by EKO at 12:01 pm on 18 June 2020 and 12:10 pm on 13

December 2020), respectively. Afterwards, PWV and AOD were inverted on these spectrums using the method described in
185 Section 3, taking the standard deviation of the inversion values as the uncertainty of the inversions.

Table 3 MS711 and MS712 calibration uncertainty

Spectroradiometer	Wavelength range	Uncertainty
MS711	300 nm – 350 nm	±17.4 %
	350 nm – 450 nm	±5.1 %
	450 nm – 1050 nm	±4.2 %
	1050 nm – 1100 nm	±5.3 %
MS712	900 nm – 950 nm	±4.52 %
	950 nm – 1600 nm	±4.84 %
	1600 nm – 1700 nm	±23.67 %
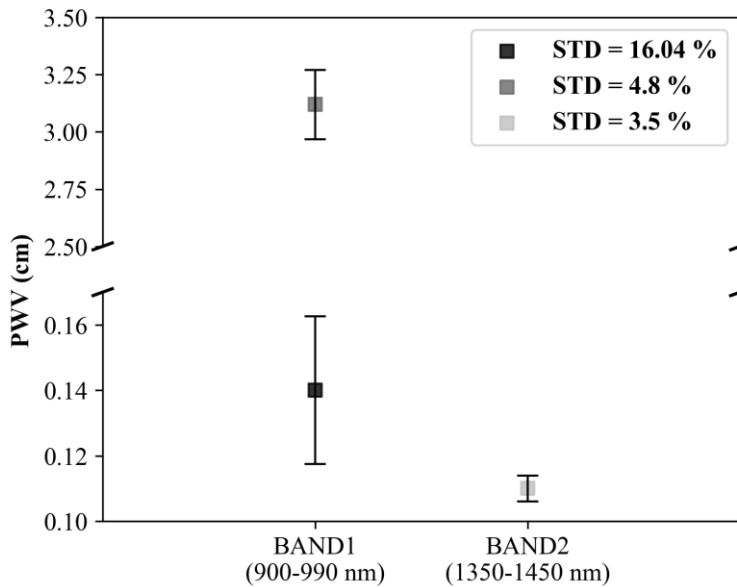
Figure 7. Mean and error bars of the PWV retrievals obtained using BAND1 and BAND2 based on the method described in Sect.
190 **3.2 for the spectral curves after overlaying the calibration uncertainties.**

Figure 7 shows the mean and error bars of the PWV retrievals using BAND1 and BAND2. The uncertainty of BAND1
inversions is 4.8 % at high water vapor content and 16.04 % at low water vapor content, the uncertainty of BAND2
inversions at low water vapor content is 3.5 %. As can be seen, in the case of low water vapor content, the uncertainty of the
195 PWV inversion values of BAND1 are significantly larger than that of the rich water vapor content, but the uncertainty of the
PWV inversion values of BAND2 are still lower.
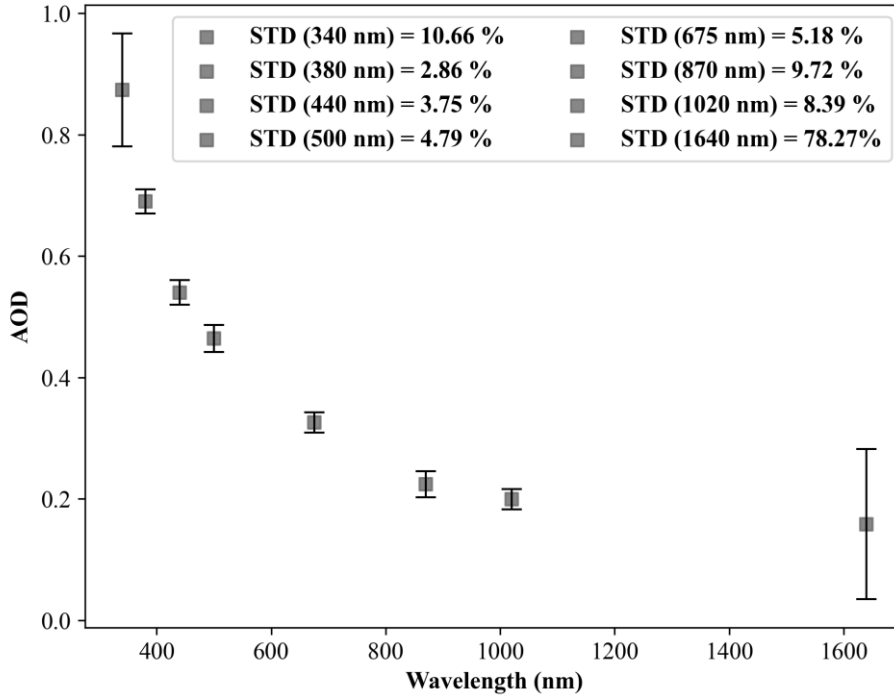
Figure 8. Mean and error bars of AOD at the wavelengths corresponding to the CE-318 filters obtained using the method described in Section 3.3 for the spectral curves after overlaying the calibration uncertainties.

200

Figure 8 plots the uncertainties of the AOD retrievals at the wavelengths corresponding to the CE-318 filters. In general, the uncertainties of aerosol inversions are low in the visible band, and increase in the near-infrared band. In addition, it can be seen from the figure that the uncertainties of the AOD retrievals of the EKO instruments at 340nm and 1640nm are very large. Presumably due to the large calibration uncertainty of the EKO instruments at these two wavelengths, so the AOD

205   retrievals of these two wavelengths are not recommended.

5 Results

The measurements of MS711 and MS712 from June 2020 to March 2021 at the top of IAP's building are used to derive the PWV and AOD, the space-time synchronized CE318 data are used as reference, the number of matching data points is 5008. The mean deviation and variance between the results of the two instruments are given by:

210   $$\overline{X} = \frac{1}{n}\sum_i \left(X_{EKO}^i - X_{cimel}^i\right) ,$$ (11)

$$\delta_X = \sqrt{\frac{1}{n}\sum_i \left(X_{EKO}^i - X_{cimel}^i\right)^2} ,$$ (12)

where X is either PWV or AOD, the subscript denotes EKO instruments or CE-318.
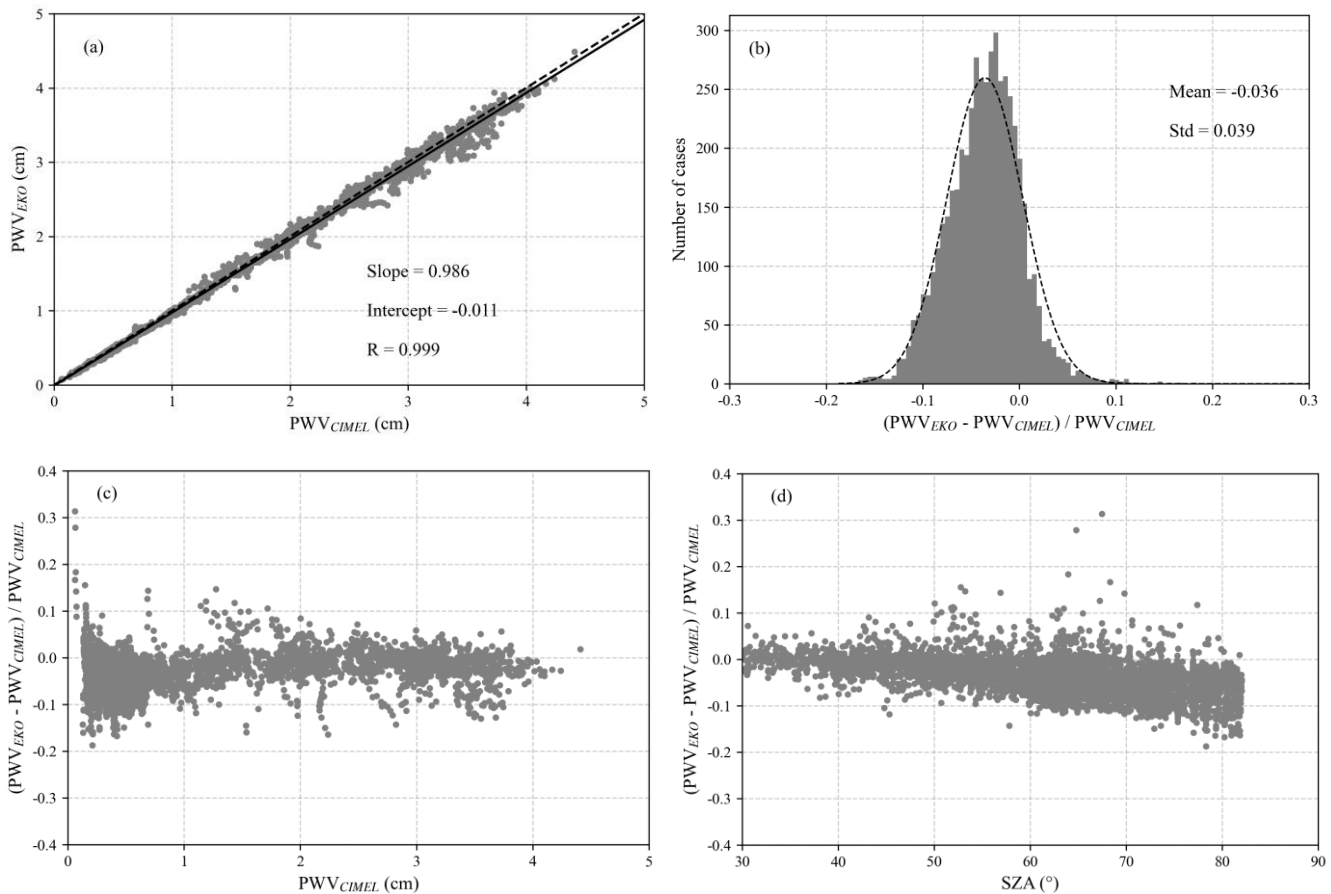
215

Figure 9. PWV retrievals from EKO using the spectral approach in the 880–1000 nm region compared to the synchronous data of CE-318 in the measuring period (a), histogram of relative difference among PWV_EKO and PWV_CIMEL (b), and the relative difference plotted against PWV_CIMEL (c) and solar zenith angle (d).

220   The PWV retrievals using the band near 940 nm of EKO and CE-318 are shown in Fig. 9. It reveals that the retrievals of EKO have a high consistency with those of CE-318, the correlation coefficient is 0.999, the mean bias and the standard deviation are of -0.027 cm (-3.57 %) and 0.054 cm (3.93 %), respectively, the relative differences for 95 % of the retrievals are between -0.114 and 0.042. Further analysis found that the differences depend on the solar elevation angle, the lower sun position, the larger difference. This is because in the case of a low solar elevation angle, the light intensity is very weak and

225   the light path is long, which is easy to be limited by the signal-to-noise ratio of the instrument, and the inversion results may have large deviations, which also occurs in AOD inversion using other spectroradiometer (Kazadzis et al., 2014). In addition, as can be seen from Table 4, the relative deviations of the PWV obtained by BAND1 (near 940 nm) varied from -2.67 % to -

4.90 % with decreasing water vapor content (PWV < 0.5 cm), which may be due to the increased uncertainty in PWV retrievals of the dry atmosphere.
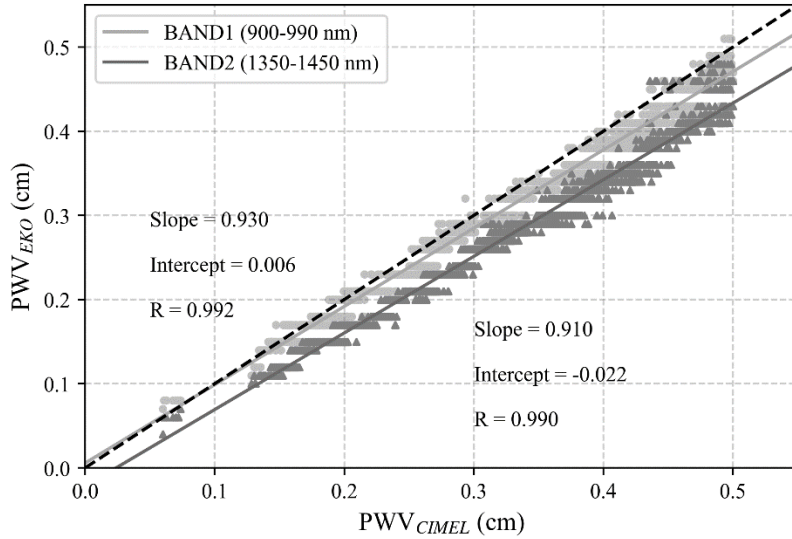
230

Figure 10. Comparison of water vapor retrieved from BAND1 and BAND2 with PWV$_{CIMEL}$ when PWV$_{CIMEL}$ is less than 0.5 cm.

Table 4 Statistics of the comparison between PWV$_{EKO}$ and the PWV$_{CIMEL}$. (N: number of data, R: Pearson correlation coefficient, Slope: slope of the least squares fit between PWV$_{EKO}$ and PWV$_{CIMEL}$, RMSE: root mean square error, MB: mean bias, STD: standard deviation).

CE-318/EKO	BAND	N	R	Slope	RMSE (cm)	MB (cm)	STD (cm)
All data	BAND1	5008	0.999	0.986	0.061 (5.31 %)	-0.027 (-3.57 %)	0.054 (3.93 %)
PWV$_{CIMEL}$>0.5 cm	BAND1	2977	0.998	0.985	0.077 (4.41 %)	-0.034 (-2.67 %)	0.069 (3.50 %)
PWV$_{CIMEL}$<0.5 cm	BAND1	2031	0.992	0.930	0.022 (6.41 %)	-0.017 (-4.90 %)	0.014 (4.13 %)
	BAND2	2031	0.990	0.910	0.054 (16.79 %)	-0.051 (-16.26 %)	0.016 (4.17 %)

235

Figure 10 shows the water vapor retrievals of BAND1 and BAND2 for dry atmosphere, their statistics are also presented in Table 4. The results of BAND1 are relatively higher than those of BAND2, which is consistent with the inversion test results in Fig. 5, indicating that the PWV retrievals of the band near 940 nm are closer to AERONET, but the PWV inversion using the band near 1370 nm may be more accurate for dry atmosphere.
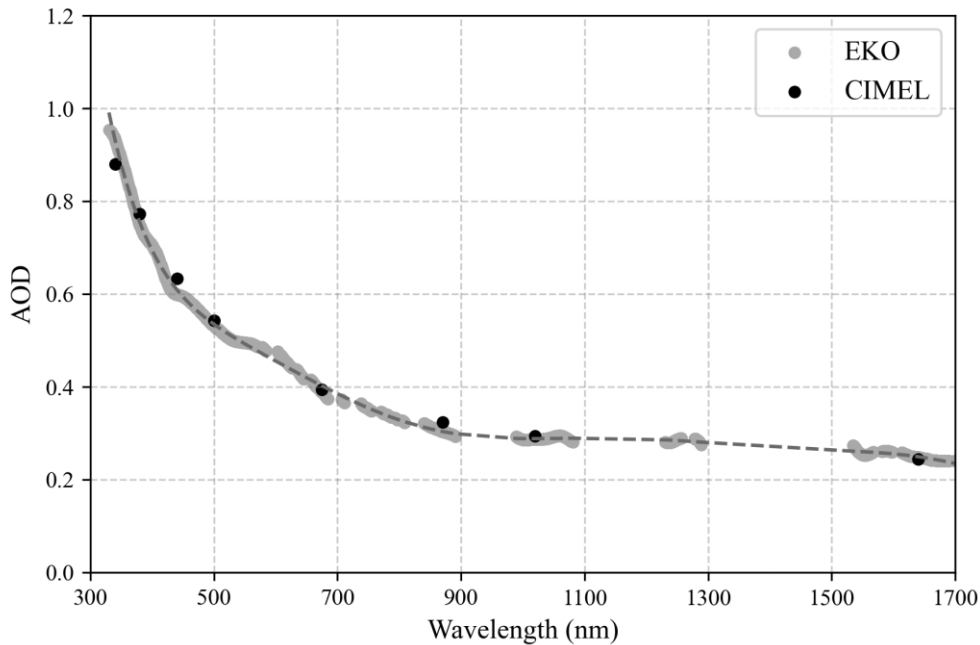
240

Figure 11. The AOD was retrieved by EKO and provided by AERONET CE-318 on 06 June 2020 (15:22 UTC+8), the dashed line is the spectral AOD obtained by the AOD_{EKO} high-order fitting.

Figure 11 shows an example of AOD_{EKO}, the AOD derived from EKO instruments is very close to the CE-318 data. The

245 spectral AOD here is obtained by the method described in Section 3.2. It is not suitable to provide spectral AOD in the case of ignoring the absorption of other gases except water vapor, so this example is only to illustrate that EKO instruments have the potential to provide spectral AOD. The spectral AOD may provide some assistance for other trace gases retrieval.
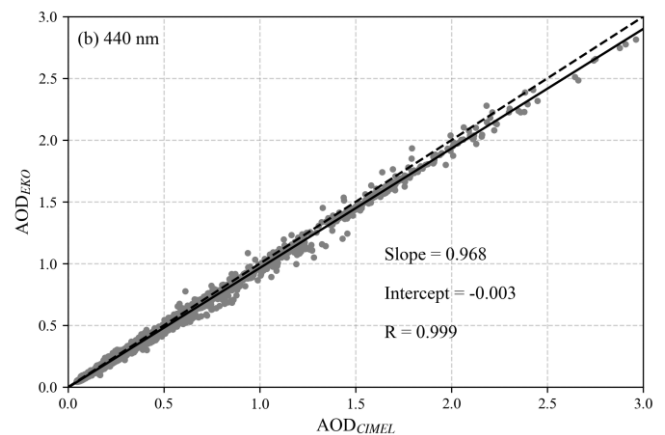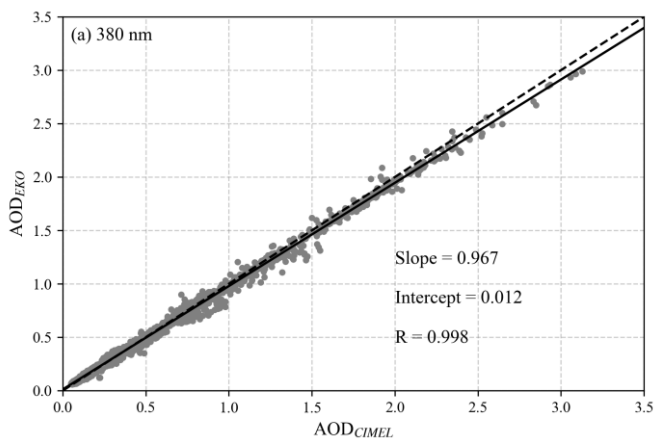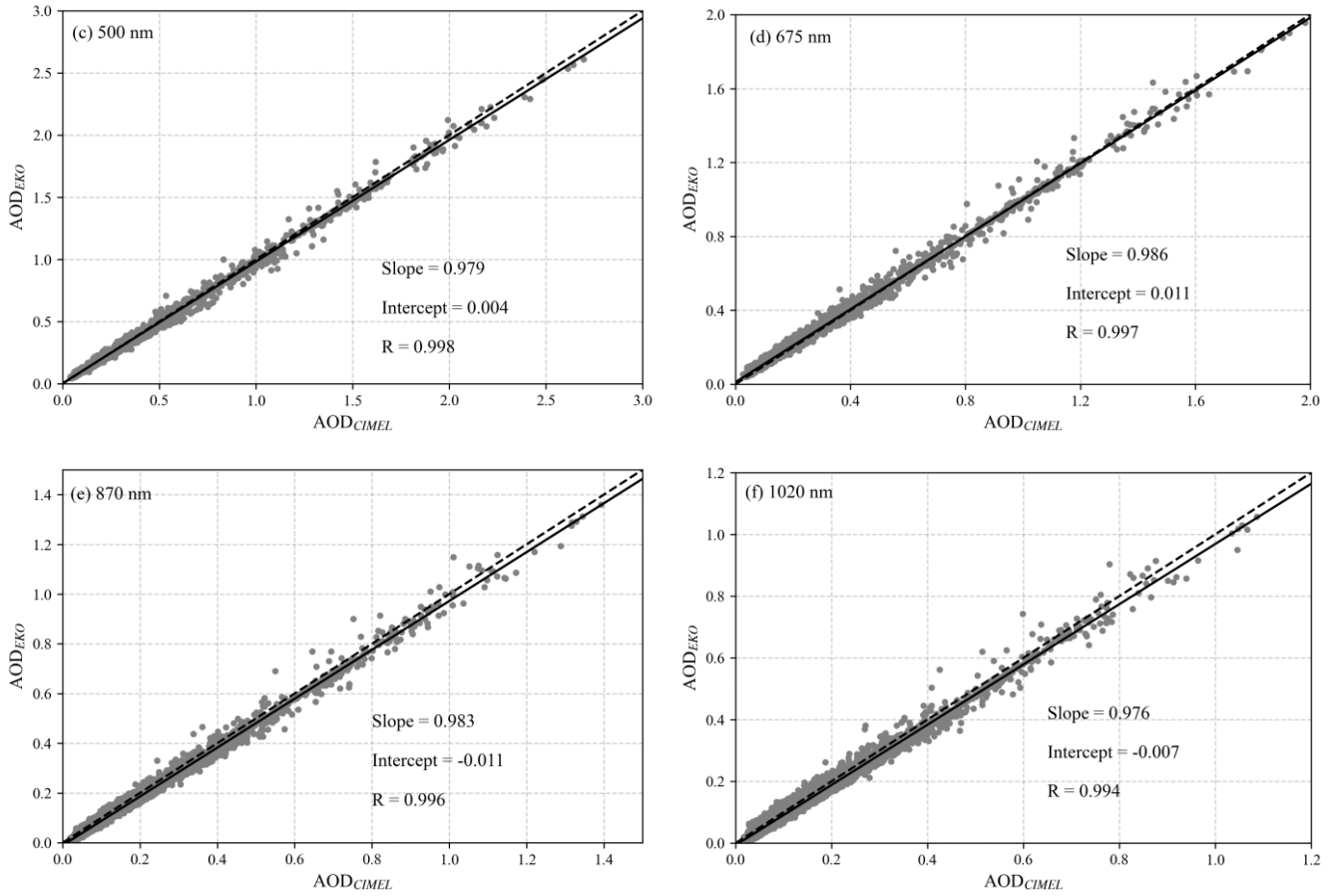
Figure 12. Comparison of AOD$_{EKO}$ versus AOD$_{CIMEL}$ at 380 nm (a), 440 nm (b), 500 nm (c), 675 nm (d), 870 nm (e) and 1020 nm (f) from June 2020 to March 2021 at IAP.

Table 5 Statistics of the comparison between AOD$_{EKO}$ and AOD$_{CIMEL}$ at 380, 440, 500, 675, 870 and 1020 nm from June 2020 to March 2021 at IAP.

Wavelength (nm)	R	Slope	RMSE	MB	STD
380	0.998	0.967	0.028 (9.16 %)	-0.002 (3.06 %)	0.028 (8.63 %)
440	0.999	0.968	0.029 (7.31 %)	-0.016 (-4.65 %)	0.024 (5.64 %)
500	0.998	0.979	0.021 (7.46 %)	-0.003 (0.69 %)	0.021 (7.42 %)
675	0.997	0.986	0.020 (17.45 %)	0.008 (9.37 %)	0.019 (14.72 %)
870	0.996	0.983	0.021 (20.01 %)	-0.014 (-13.59 %)	0.015 (14.70 %)
1020	0.994	0.976	0.019 (22.06 %)	-0.010 (-11.81 %)	0.016 (18.63 %)

To evaluate the differences between AOD$_{EKO}$ and AOD$_{CIMEL}$ ulteriorly, the AOD$_{EKO}$ in the corresponding bands of the CE-318 (380, 440, 500, 675, 870, 1020 nm) were compared and analysed (Fig. 12), the specific statistics are listed in Table 5. The AOD retrievals from the two kinds of instruments are consistent, the correlation coefficients exceed 0.99, the relative

260 differences are between -13.59 % and 9.37 %. Further analysis found that the AOD differences in the visible band were small, especially at 500 nm, the MB and RMSE were -0.003 (0.69 %) and 0.021 (7.46 %), respectively, while the differences of near-infrared band were significantly increased. According to the uncertainty analysis of AOD inversion in Sect. 4, it is probably because the uncertainties of AOD inversion are small in the visible band, but relatively large in the near-infrared band.

265
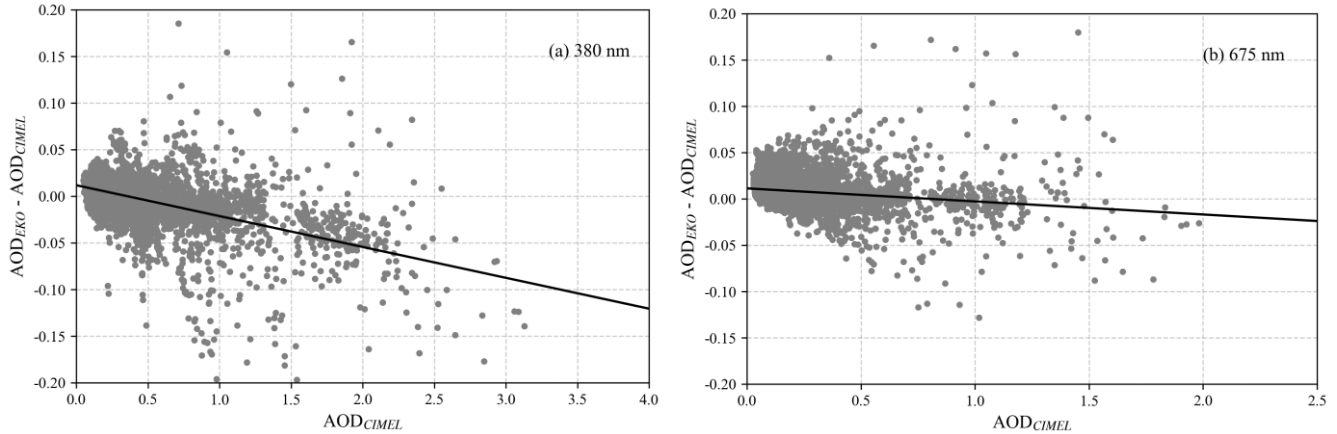
Figure 13. The Bias between synchronous AOD$_{EKO}$ and AOD$_{CIMEL}$ against AOD$_{CIMEL}$ at 380 nm (a) and 675 nm (b).

Figure 13 plots the variation of AOD difference with that of CE-318 for 380 nm and 675 nm. AOD$_{EKO}$ shows obvious
270 underestimation, especially at 380nm, which is reasonable since current AOD inversion algorithm neglect the near-forward aerosol scattering that can lead to underestimation of AOD (Sinyuk et al., 2012). The FOV of MS711 and MS712 is 5°, which is double that of the radiometer for AOD recommended by WMO and four times that of CE-318, therefore, the forward scattered photons received by MS711 and MS712 are also more than CE-318, especially for heavy aerosol loading atmosphere and shorter wavelengths. The near-forward scattering correction will be considered in the next version of the
275 algorithm.

6 Summary and Conclusions

The water vapor absorption band near 940 nm is currently used to derive the PWV commonly, and AOD from sun photometer is usually given at several wavelengths apart, which sometimes does not fully meet the needs of the application. Therefore, combined with the advantage that EKO instruments can measure the direct normal solar irradiance in the spectral
280 range of 300-1700 nm, the water vapor band near 1370 nm is also used to derive PWV for dry atmosphere, and the spectral AOD is obtained by higher-order fitting of the AOD inverted from EKO at more wavelengths. Different from the three-parameter method, the retrieval algorithm is a physical method based on MODTRAN version 4.3. Data measured by EKO

MS711 and MS712 at IAP from June 2020 to March 2021 are used for inverting PWV and spectral AOD, and the results are compared with those from the collocated CE-318.

285 We used the calibration uncertainty obtained from the instruments calibration certificate to estimate the uncertainties of the water vapor and aerosol retrievals. The uncertainty of the PWV retrievals of the band around 940 nm at high water vapor content is significantly smaller than that at low water vapor content, ranging from 4.8 % to 16.04 %. The uncertainty of the PWV retrievals of the band near 1370 nm at low water vapor content is as low as 3.5 %. The uncertainties of AOD retrievals are large at the wavelengths less than 350 nm and greater than 1600 nm, generally small in the visible band (around 5 %),

290 and relatively large in the near-infrared band (around 9 %).

The PWV retrieved from EKO instruments and CE-318 at the band near 940 nm are in good agreement, the correlation coefficient is 0.999, the mean bias, root mean square error and standard deviation are -0.027 cm (-3.57 %), 0.061 cm (5.31 %) and 0.054 cm (3.93 %), respectively. However, for dry atmosphere with PWV<0.5 cm, the retrievals at the band around 1370 nm may be more accurate than the band around 940 nm.

295 The AOD retrieved from EKO instruments also agree well with that from CE-318, the correlation coefficients are greater than 0.99, the mean bias are between -0.016 and 0.008. Due to the large FOV of the EKO instruments and the current algorithm ignoring the contribution of near-forward scattering, the AOD retrievals from EKO instruments are often slightly underestimated, especially for heavy aerosol loading and shorter wavelengths, which will be considered in the future version.

Data availability

300 Data used in this study are available from the corresponding author upon request (dmz@mail.iap.ac.cn).

Author contributions

M. Duan and C. Qiao determined the main goal of this study. C. Qiao carried it out, analysed the data, and prepared the paper with contributions from all co-authors. S. Jia provided instrumental support. P. Wang and J. Huo provided guidance on algorithmic procedures.

305 **Competing interests**

The authors declare that they have no conflict of interest.

Acknowledgements

This research is supported by the National Natural Science Foundation of China (Grant No. 42030107 and No. 42175150). We also thank all the teachers and students who participated in the discussion about this work.

References

Augustine, J. A., Hodges, G. B., Dutton, E. G., Michalsky, J. J., and Cornwall, C. R.: An aerosol optical depth climatology for NOAA's national surface radiation budget network (SURFRAD), J. Geophys. Res., 113, https://doi.org/10.1029/2007jd009504, 2008.

Barreto, A., Cuevas, E., Pallé, P., Romero, P. M., Guirado, C., Wehrli, C. J., and Almansa, F.: Recovering long-term aerosol optical depth series (1976–2012) from an astronomical potassium-based resonance scattering spectrometer, Atmos. Meas. Tech., 7, 4093-4121, https://doi.org/10.5194/amt-7-4103-2014, 2014.

Bevis, M., Businger, S., Herring, T. A., Rocken, C., Anthes, R. A., and Ware, R. H.: GPS meteorology: Remote sensing of atmospheric water vapor using the global positioning system, J. Geophys. Res.: Atmos., 97, 15787-15801, https://doi.org/10.1029/92JD01517, 1992.

Bodhaine, B. A., Wood, N. B., Dutton, E. G., and Slusser, J. R.: On Rayleigh Optical Depth Calculations, J. Atmos. Oceanic Technol., 16, 1854-1861, https://doi.org/10.1175/1520-0426(1999)016<1854:Orodc>2.0.Co;2, 1999.

Bojinski, S., Verstraete, M., Peterson, T. C., Richter, C., Simmons, A., and Zemp, M.: The Concept of Essential Climate Variables in Support of Climate Research, Applications, and Policy, Bull. Am. Meteorol. Soc., 95, 1431-1443, https://doi.org/10.1175/bams-d-13-00047.1, 2014.

Cachorro, V. E., Berjon, A., Toledano, C., Mogo, S., Prats, N., Frutos, M. D., Vilaplana, J. M., Sorribas, M., Morena, B. A. D. L., and Groebner, J.: Detailed Aerosol Optical Depth Intercomparison between Brewer and Li-Cor 1800 Spectroradiometers and a Cimel Sun Photometer, J. Atmos. Oceanic Technol., 26, 1558-1571, https://doi.org/10.1175/2009JTECHA1217.1, 2009.

Campanelli, M., Estelles, V., Smyth, T., Tomasi, C., and Nakajima, T.: Monitoring of Eyjafjallajoekull volcanic aerosol by the new European SkyRad users (ESR) sun-sky radiometer network, Atmos. Environ., 48, 33-45, https://doi.org/10.1016/j.atmosenv.2011.09.070, 2012.

Campanelli, M., Nakajima, T., Khatri, P., Takamura, T., Uchiyama, A., Estelles, V., Liberti, G. L., and Malvestuto, V.: Retrieval of characteristic parameters for water vapour transmittance in the development of ground-based sun–sky radiometric measurements of columnar water vapour, Atmos. Meas. Tech., 7, 1075-1087, https://doi.org/10.5194/amt-7-1075-2014, 2014.

Che, H., Gui, K., Chen, Q., Zheng, Y., Yu, J., Sun, T., Zhang, X., and Shi, G.: Calibration of the 936 nm water-vapor channel for the China aerosol remote sensing NETwork (CARSNET) and the effect of the retrieval water-vapor on aerosol optical property over Beijing, China, Atmos. Pollut. Res., 7, 743-753, https://doi.org/10.1016/j.apr.2016.04.003, 2016.

Cuevas Agulló, E., Milford, C., and Tarasova, O.: Izaña Atmospheric Research Center. Activity Report 2012-2014, https://doi.org/10.31978/281-15-004-2, 2015.

Dubovik, O., Li, Z., Mishchenko, M. I., Tanré, D., Karol, Y., Bojkov, B., Cairns, B., Diner, D. J., Espinosa, W. R., Goloub, P., Gu, X., Hasekamp, O., Hong, J., Hou, W., Knobelspiesse, K. D., Landgraf, J., Li, L., Litvinov, P., Liu, Y., Lopatin, A.,

Marbach, T., Maring, H., Martins, V., Meijer, Y., Milinevsky, G., Mukai, S., Parol, F., Qiao, Y., Remer, L., Rietjens, J., Sano, I., Stammes, P., Stamnes, S., Sun, X., Tabary, P., Travis, L. D., Waquet, F., Xu, F., Yan, C., and Yin, D.:

345   Polarimetric remote sensing of atmospheric aerosols: Instruments, methodologies, results, and perspectives, J. Quant. Spectrosc. Radiat. Transfer, 224, 474-511, https://doi.org/10.1016/j.jqsrt.2018.11.024, 2019.

Estellés, V., Utrillas, M. P., Martínez-Lozano, J. A., Alcántara, A., Alados-Arboledas, L., Olmo, F. J., Lorente, J., de Cabo, X., Cachorro, V., Horvath, H., Labajo, A., Sorribas, M., Díaz, J. P., Díaz, A. M., Silva, A. M., Elías, T., Pujadas, M., Rodrigues, J. A., Cañada, J., and García, Y.: Intercomparison of spectroradiometers and Sun photometers for the

350   determination of the aerosol optical depth during the VELETA-2002 field campaign, J. Geophys. Res., 111, https://doi.org/10.1029/2005jd006047, 2006.

García, R. D., Cuevas, E., Barreto, Á., Cachorro, V. E., Pó, M., Ramos, R., and Hoogendijk, K.: Aerosol retrievals from the EKO MS-711 spectral direct irradiance measurements and corrections of the circumsolar radiation, Atmos. Meas. Tech., 13, 2601-2621, https://doi.org/10.5194/amt-13-2601-2020, 2020.

355   García, R. D., Cuevas, E., Cachorro, V. E., García, O. E., Barreto, Á., Almansa, A. F., Romero-Campos, P. M., Ramos, R., Pó, M., Hoogendijk, K., and Gross, J.: Water Vapor Retrievals from Spectral Direct Irradiance Measured with an EKO MS-711 Spectroradiometer—Intercomparison with Other Techniques, Remote Sens., 13, https://doi.org/10.3390/rs13030350, 2021.

Gueymard, C. A.: Parameterized transmittance model for direct beam and circumsolar spectral irradiance, Sol. Energy, 71,

360   325-346, https://doi.org/10.1016/S0038-092X(01)00054-8, 2001.

Güldner, J. and Spänkuch, D.: Remote Sensing of the Thermodynamic State of the Atmospheric Boundary Layer by Ground-Based Microwave Radiometry, J. Atmos. Oceanic Technol., 18, 925-933, https://doi.org/10.1175/1520-0426(2001)018<0925:Rsotts>2.0.Co;2, 2001.

Hansen, J. E. and Travis, L. D.: Light scattering in planetary atmospheres, Space Sci. Rev., 16, 527-610,

365   https://doi.org/10.1007/BF00168069, 1974.

Holben, B. N., Eck, T. F., Slutsker, I., Tanré, D., Buis, J. P., Setzer, A., Vermote, E., Reagan, J. A., Kaufman, Y. J., and Nakajima, T.: AERONET—A Federated Instrument Network and Data Archive for Aerosol Characterization, Remote Sens. Environ., 66, 1-16, https://doi.org/10.1016/S0034-4257(98)00031-5, 1998.

Ingold, T., Schmid, B., Mätzler, C., Demoulin, P., and Kämpfer, N.: Modeled and empirical approaches for retrieving

370   columnar water vapor from solar transmittance measurements in the 0.72, 0.82, and 0.94 μm absorption bands, J. Geophys. Res.: Atmos., 105, 24327-24343, https://doi.org/10.1029/2000jd900392, 2000.

IPCC: The Physical Science Basis. Intergovernmental Panel on Climate Change, https://doi.org/10.1017/CBO9781107415324, 2013.

IPCC: Climate Change 2021: The Physical Science Basis. Contribution of Working Group I to the Sixth Assessment Report

375   of the Intergovernmental Panel on Climate Change, https://doi.org/10.1017/9781009157896, 2021.

J. and Güldner: A model-based approach to adjust microwave observations for operational applications: results of a campaign at Munich Airport in winter 2011/2012, Atmos. Meas. Tech., 6, 2879-2891, https://doi.org/10.5194/amt-6-2879-2013, 2013.

Kaufman, Y. J., Tanré, D., and Boucher, O.: A satellite view of aerosols in the climate system, Nature, 419, 215-223,
380   https://doi.org/10.1038/nature01091, 2002.

Kazadzis, S., Kouremeti, N., Diémoz, H., Gröbner, J., and Wehrli, C.: Results from the Fourth WMO Filter Radiometer Comparison for aerosol optical depth measurements, Atmos. Chem. Phys., 1-27, https://doi.org/10.5194/acp-2017-1105, 2018a.

Kazadzis, S., Kouremeti, N., Nyeki, S., Gröbner, J., and Wehrli, C.: The World Optical Depth Research and Calibration
385   Center (WORCC) quality assurance and quality control of GAW-PFR AOD measurements, Geosci. Instrum. Method. Data Syst., 7, 39-53, https://doi.org/10.5194/gi-7-39-2018, 2018b.

Kazadzis, S., Veselovskii, I., Amiridis, V., Gr?Bner, J., Suvorina, A., Nyeki, S., Gerasopoulos, E., Kouremeti, N., Taylor, M., and Tsekeri, A.: Aerosol microphysical retrievals from precision filter radiometer direct solar radiation measurements and comparison with AERONET, Atmos. Meas. Tech., 7, 2013– 2025, https://doi.org/10.5194/amt-7-2013-2014, 2014.

390   Kokhanovsky, A. A.: Remote sensing of atmospheric aerosol using spaceborne optical observations, Earth Sci. Rev., 116, 95-108, https://doi.org/10.1016/j.earscirev.2012.10.008, 2013.

Kurucz, R. L.: Synthetic Infrared Spectra, Infrared Solar Physics, 523-531, https://doi.org/10.1007/978-94-011-1926-9_62, 1994.

Larar, A. M., Berk, A., Anderson, G. P., Bernstein, L. S., Acharya, P. K., Dothe, H., Matthew, M. W., Adler-Golden, S. M.,
395   Chetwynd, J. J. H., Richtsmeier, S. C., Pukall, B., Allred, C. L., Jeong, L. S., and Hoke, M. L.: MODTRAN4 radiative transfer modeling for atmospheric correction, Optical Spectroscopic Techniques and Instrumentation for Atmospheric and Space Research III, https://doi.org/10.1117/12.366388, 1999.

Li, C., Li, J., Xu, H., Li, Z., Xia, X., and Che, H.: Evaluating VIIRS EPS Aerosol Optical Depth in China: An intercomparison against ground-based measurements and MODIS, J. Quant. Spectrosc. Radiat. Transfer, 224, 368-377,
400   https://doi.org/10.1016/j.jqsrt.2018.12.002, 2019.

Li, Z. Q., Xu, H., Li, K. T., Li, D. H., Xie, Y. S., Li, L., Zhang, Y., Gu, X. F., Zhao, W., Tian, Q. J., Deng, R. R., Su, X. L., Huang, B., Qiao, Y. L., Cui, W. Y., Hu, Y., Gong, C. L., Wang, Y. Q., Wang, X. F., Wang, J. P., Du, W. B., Pan, Z. Q., Li, Z. Z., and Bu, D.: Comprehensive Study of Optical, Physical, Chemical, and Radiative Properties of Total Columnar Atmospheric Aerosols over China: An Overview of Sun–Sky Radiometer Observation Network (SONET) Measurements,
405   Bull. Am. Meteorol. Soc., 99, 739-755, https://doi.org/10.1175/bams-d-17-0133.1, 2018.

Michalsky, J. J., Schlemmer, J. A., Berkheiser, W. E., Berndt, J. L., Harrison, L. C., Laulainen, N. S., Larson, N. R., and Barnard, J. C.: Multiyear measurements of aerosol optical depth in the Atmospheric Radiation Measurement and Quantitative Links programs, J. Geophys. Res.: Atmos., 106, 12099-12107, https://doi.org/10.1029/2001jd900096, 2001.

NOAA: US standard atmosphere, National Oceanic and Atmospheric Administration1976.

410 Ramachandran, S., Jayaraman, A., Acharya, Y., and Subbaraya, B.: Features of aerosol optical depths over Ahmedabad as observed with a Sun-tracking photometer, Beitr. Phys. Atmosph., 67, 1994.

Raptis, P.-I., Kazadzis, S., Gröbner, J., Kouremeti, N., Doppler, L., Becker, R., and Helmis, C.: Water Vapor Retrieval using the Precision Solar Spectroradiometer, Atmos. Meas. Tech., 1143–1157, https://doi.org/10.5194/amt-2017-370, 2018.

Schmid, B., Michalsky, J., Halthore, R., Beauharnois, M., Harrison, L., Livingston, J., Russell, P., Holben, B., Eck, T., and
415 Smirnov, A.: Comparison of aerosol optical depth from four solar radiometers during the fall 1997 ARM intensive observation period, Geophys. Res. Lett., 26, 2725-2728, https://doi.org/10.1029/1999gl900513, 1999.

Sinyuk, A., Holben, B. N., Smirnov, A., Eck, T. F., Slutsker, I., Schafer, J. S., Giles, D. M., and Sorokin, M.: Assessment of error in aerosol optical depth measured by AERONET due to aerosol forward scattering, Geophys. Res. Lett., 39, 23806, https://doi.org/10.1029/2012gl053894, 2012.

420 Smirnov, A., Holben, B., Lyapustin, A., Slutsker, I., and Eck, T.: AERONET processing algorithms refinement, AERONET Workshop, El Arenosillo, Spain, 10-14, 291795812, 2004.

Smirnov, A., Holben, B. N., Eck, T. F., Dubovik, O., and Slutsker, I.: Cloud-Screening and Quality Control Algorithms for the AERONET Database, Remote Sens. Environ., 73, 337-349, https://doi.org/10.1016/s0034-4257(00)00109-7, 2000.

Stamnes, K., Tsay, S. C., Wiscombe, W. J., and Jayaweera, K.: Numerically stable algorithm for discrete-ordinate-method
425 radiative transfer in multiple scattering and emitting layered media, Appl. Optics, 27, 2502-2509, https://doi.org/10.1364/AO.27.002502, 1988.

Swinehart, F. D.: The Beer-Lambert Law, J. Chem. Educ., 39, 333, https://doi.org/10.1021/ed039p333, 1962.

Wang, J., Zhang, L., Dai, A., Van Hove, T., and Van Baelen, J.: A near-global, 2-hourly data set of atmospheric precipitable water from ground-based GPS measurements, J. Geophys. Res., 112, https://doi.org/10.1029/2006jd007529, 2007.

430 Wehrli, C.: Calibrations of filter radiometers for determination of atmospheric optical depth, Metrologia, 37, 419, https://doi.org/10.1088/0026-1394/37/5/16, 2003.

WMO: WMO/GAW Experts Workshop on a Global Surface-Based Network for Long Term Observations of Column Aerosol Optical Properties, GAW Report No. 162, WMO TD No. 1287, available at: https://library.wmo.int/doc_num.php?explnum_id=9299 (last access: 6 May 2022), 2005.

435 WMO: GAW Report-No 231, Fourth WMO Filter Radiometer Comparison (FRC-IV), Davos, Switzerland, 28 September– 16 October 2015, WMO, available at: https://library.wmo.int/doc_num.php?explnum_id=3369 (last access: 6 May 2022), 2016.